Published in final edited form as:
Appl Phys B. 2007 March ; 87(1): 37–44. doi:10.1007/s00340-006-2545-y.

Raman effects in the infrared supercontinuum generation in soft-glass PCFs

V.L. Kalashnikov[1], **E. Sorokin**[1], and **I.T. Sorokina**[1]
[1] Institut für Photonik, TU Wien, Gusshausstr. 27/387, A-1040 Vienna, Austria

Abstract

Measurements of the Raman gain spectra in the SF6 and SF57 highly-nonlinear-glasses demonstrated twice as high Raman shift in comparison with the fused silica. Numerical simulation predicted that a large Raman shift in combination with high nonlinearity can significantly reduce the required input pulse intensity for supercontinuum in these glasses, retaining the necessary degree of coherence. We found, that the degradation of the SC coherence due to Raman soliton jitter can be effectively controlled by a correct choice of input intensity and fiber length. Also it was found, that high degree of coherence correlates with the spectrum shape in the vicinity of the Raman threshold, providing an convenient experimental observable.

1 Introduction

Over-octave spanning infrared (IR) spectral supercontinua (SC) are of interest for frequency metrology and high-resolution spectroscopy [1], femtosecond pulse stabilization [2] and ultra-short pulse compression [3]. In contrast to bulk materials and gases [4], photonic crystal fibers (PCFs) and tapered fibers have allowed reducing the SC generation threshold down to sub-1 nJ input energies [5]. Such a low-threshold spectral extra-broadening results from two main sources: i) strong mode confinement inside a μm-sized fiber core and ii) precisely controllable contribution of the mode group-delay dispersion (GDD) of a fiber. Mode confinement enhances the nonlinearity in agreement with the formula for the self-phase modulation coefficient [6]: $\gamma = n_2\omega/c\, A_{eff}$, where n_2 is the nonlinear refraction coefficient, ω is the carrier frequency, c is the light velocity, A_{eff} is the effective mode aria. The GDD control allows operating in the vicinity of zero-dispersion wavelength (ZDW) that puts in action the soliton fission mechanism of the SC formation [7].

However, the above mechanisms reducing the SC threshold become less efficient with the wavelength increase into the infrared. Firstly, the effective nonlinearity scales as $\gamma \propto 1/\lambda^3$ [8]. Secondly, the core size must become larger if ZDW is to be shifted to the IR. The latter additionally decreases the effective nonlinearity and can lead to multimode intra-fiber pulse propagation [8].

There are two main ways to compensate the effective nonlinearity decrease in IR-region. The GDD flattening in the vicinity of ZDW allows longer nonlinear propagation lengths for PCFs with $\gamma = 20 \div 30$ W^{-1}km^{-1}. As a result, the spectrum broadens due to the radiation of a dispersion wave dispersion [14] and the soliton self-frequency shift [9-11]. For the latter, the dependence $\Delta\omega \propto (\gamma E)^4 L/|\beta_2|^3$ [6] means that small GDD coefficient β_2 within a wide spectral range as well as a long propagation length L result in a large self-frequency shift $\Delta\omega$ even for the moderate pulse energy E.

Correspondence to: kalashnikov@tuwien.ac.at.

Europe PMC Funders Author Manuscripts

Another way is to use PCF with high nonlinear refractivity, e.g. SF6 glass ($\gamma = 115$ $W^{-1}km^{-1}$ if ZDW is shifted to 1.5 μm, see below) [8,12,13]. In this case, the spectrum is broadened by the soliton fission mechanism [7]. Effectiveness of the SC generation from such a fiber pumped by a Cr:YAG oscillator was demonstrated in Ref. [8]. Role of SRS in the SC formation for highly-nonlinear PCFs (like SF6 glass [8]) in the vicinity of ZDW remains unexplored.

SRS-induced enhancement of the spectral extra-broadening can be considered as a very important factor, which would be able to compensate the effective nonlinearity decrease in IR-region. However, a stumbling block is the spectral phase coherence, which can degrade due to SRS induced spectral and timing jitters of a soliton [15]. The problem of noise limitations on the SC generation [16] is significant for metrology and femtosecond pulse phase stabilization. Frequency-doubled and tripled (within SC) frequency components can give an information about the femtosecond pulse carrier envelope phase only if the corresponding spectral components belong to the spectral windows, where a coherence is close to unity. However, such a coherence can be essentially degraded within the SC spectrum [16,17]. The spectral phase coherence is thus a crucial factor in an analysis of the IR supercontinua.

In this work we demonstrate that SRS in the highly nonlinear glasses (SF6 and SF57) produces an approximately doubled frequency shift in comparison with that in common (fused-silica based) telecommunication fibers. As a result, the octave-spanning SC can be produced by sub-200 pJ 60 fs pulses from an all-solid-state Cr:YAG oscillator [18]. We show that the spectral coherence degradation can be significantly reduced (almost without the SC width reduction) by the fiber length optimization, and provide an observable criterium for high-coherence operation. We also show that the spectral coherence degradation due to Raman soliton jitter does not impose a limitation on the maximum spectral coherence in the quantum limit.

2 Measurements of the Raman gain for SF6 and SF57 glasses

The absolute measurements of Raman gain g_R for the nonlinear glasses of interest are not available. It is possible, however, to use the spectra of spontaneous Raman scattering to estimate g_R. We make use of the fact, that [35]

$$g_R \propto \frac{\mathrm{Im}\chi^{(3)}}{\lambda n^2}, \quad \sigma_R \propto \frac{\mathrm{Im}\chi^{(3)}}{\lambda^2 n^2}, \quad (1)$$

where $\chi^{(3)}$ is the third-order susceptibility, σ_R is the integral spontaneous scattering efficiency and we neglect the difference between the refractive indices and wavelengths for the incident and scattered light. Given the spontaneous Raman spectra of a crystal with known g_R were measured under the same conditions as the unknown ones, the relations (1) allow estimating the g_R in absolute units. Since the electronic transitions are sufficiently far from the wavelength involved, the susceptibility tensors and refractive indices can be safely assumed to be wavelength independent, and the simple recalibration (1) applies (for detailed discussion, see Ref. [39])

For Raman measurements we used crystalline quartz and fused silica as reference, since the Raman gain is known for these materials [36,37]. The experimental setup implemented confocal 180° polarized scattering scheme [38] at 1545 nm. In the tightly focused confocal scheme the backscattered light is collected from a well-defined small volume about 100 μm under the surface of the sample. This allows comparing the absolute values of scattering cross-section from samples with different index of refraction, thickness, and surface quality. The back-scattering geometry provides an additional advantage in our case since it allows

accessing those components of the scattering tensor, which would be responsible for the stimulated Raman scattering interaction during the propagation. For the same reason, we measure only the polarized spectra in parallel polarizations of the input and scattered light.

Using the relations (1) and g_R of crystalline quartz and fused silica, we then calibrate the spontaneous Raman spectra yielding the g_R value at our wavelength of interest. Table 1 summarizes the results at 1.5 μm.

The Raman spectra of both SF6 and SF57 glasses are very similar, as the glasses have very close PbO-SiO_2 composition, differing only by the PbO content (Fig. 1). The absolute values of peak Raman gain in flint glasses are 6-9 times larger than that of fused silica, however the ratio of the integrated Raman gain to the electronic nonlinearity f is about the same, changing from 0.19 for fused silica to 0.13 and 0.10 for SF6 and SF57, respectively. Our measurements roughly correspond to a spectrum, provided in Ref. [40] for SF6 glass, using benzene calibration.

More important, however, is the wavelength shift between the main spectral features of the flint glasses and the fused silica. In the former, the main line around 1000 cm^{-1} corresponds to the vibrations of the isolated SiO_4 tetrahedra. In fused silica, where there are no isolated SiO_4 complexes, the Raman spectrum is concentrated around 450 cm^{-1}, corresponding to the symmetric stretch modes of the closely packed mesh of Si-O-Si bridges. As will be seen later, the twice as large Raman shift of the flint glasses can make a significant difference in the femtosecond SC generation as compared to fused silica, even though the relative contribution of the Raman nonlinearity in these glasses is lower.

3 Pulse propagation modelling

We base the analysis of the SC formation on the well-known generalized nonlinear Schrödinger equation (see, for example, [6]). In order to take into account the quantum noise effects, a quantized version of this equation is required, leading to the operator evolution equation (in the Heisenberg picture) with the corresponding commutators [19]. This equation for the photon creation and annihilation operators has to be supplemented by equations for the photon and phonon baths governing the loss and scattering processes. The resulting nonlinear system of the operator equations cannot be solved self-consistently in the general case. A powerful method to consider this problem numerically is a correspondence between the quantum operators and the classical phase-space functions (for an overview see [20]). Thus, the phase-space representations of the quantum nonlinear optics are most usable for our aims [21,22].

The Wigner representation leads to the stochastic nonlinear generalized Schrödinger equation [21,24]:

$$\begin{aligned}\frac{\partial}{\partial\zeta}\phi(\tau,\zeta) = i\left[\mp\frac{\beta(\omega)}{2}\frac{\partial^2}{\partial\tau^2}\phi - (1-f)\left(1+\frac{i}{\omega_0}\frac{\partial}{\partial\tau}\right)|\phi|^2\phi\right] \\ -if\left(1+\frac{i}{\omega_0}\frac{\partial}{\partial\tau}\right)\phi\int_{-\infty}^{\tau}d\tau' h\left(\tau-\tau'\right)|\phi\left(\tau'\right)|^2 + i\phi\Gamma,\end{aligned} \quad (2)$$

where ϕ is the photon field amplitude so that $|\phi|^2$ is normalized to the typical number of photons in an input pulse with the soliton number N: $\bar{n} \equiv c|\beta_2|A_{eff}N^2/n_2\hbar\omega_0^2 t_0$ (n_2 is the nonlinear refraction coefficient, ω_0 is the central frequency of an input pulse, t_0 is the input pulse width, β_2 is the GDD coefficient at ω_0, A_{eff} is the effective fiber mode area, c is the velocity of light). Propagation length ζ is normalized to the dispersion length $t_0^2/|\beta_2|$ and the local time τ is normalized to t_0. $\beta(\omega)$ gives dependence of the GDD coefficient on the frequency so that ω is the deviation from ω_0 and "–"-sign corresponds to an anomalous

dispersion. f is the Raman fraction in the total self-phase modulation, $h(\tau)$ is the Raman response function. Γ is the stochastic source due to photon-phonon scattering (see next section).

Strong mode confinement caused by a large refractive index reduces the wavelength dependence of A_{eff}. For the considered SF6 fiber, $A_{eff} \approx 9$ and 10 μm^2 at 1 and 2 μm wavelengthes, respectively. Therefore we did not take into account the corrections of the effective nonlinearity due to wavelength-dependence of A_{eff} [25].

To describe the SRS we have used the "homogeneous gain" approximation instead of continuum of the narrow phonon resonances [21]. Then $h(\tau)$ can be expressed through the Green's function of the damped harmonic oscillator [23]:

$$h(\tau) = \frac{T_1^2 + T_2^2}{T_1 T_2^2} \exp\left(-\frac{\tau}{T_2}\right) \sin\left(\frac{\tau}{T_1}\right), \quad (3)$$

and $T_1 = 5.5$ fs, $T_2 = 32$ fs for both SF6 and SF57. These parameters correspond to approximating the Raman spectrum of Fig. 1 by a single Lorentzian peak. f can be found from the Kramers-Kronig relation [23]:

$$f = \frac{\lambda}{2\pi^2 n_2} \int_0^\infty \frac{g_R(\omega)}{\omega} d\omega. \quad (4)$$

Eq. (2) was solved by the symmetrized split-step Fourier method. The time and propagation steps were chosen to be equal to 1 fs and 1/1000-part of the nonlinear length, respectively. The local time mesh contained 2^{15} points. An initial pulse was a *sech*-shaped pulse with $1.76 \times t_0 = 60$ fs duration centered at 1.5 μm wavelength.

4 Raman contribution

In this section we shall concentrate at an influence of SRS on the SC generation in the highly-nonlinear PCFs (in contrast to Ref. [8], where SRS was neglected). For this, a deterministic version of Eq. (2) (i.e. the classical generalized nonlinear Schrödinger equation) is appropriate.

As the high-order soliton fission mechanism reduces the SC threshold essentially [7], an immediate proximity of β_2 to zero has to be considered as a key factor, which defines the PCF geometry. For distinctness's sake, PCFs with a cylindrical core are considered.

Fig. 2 demonstrates that SF6 and SF57 glasses provide the near-zero GDD, the comparatively small third-order dispersion and the minimum core radii at $\lambda = 1.5$ μm in comparison with the another fibers under consideration. By reasons of this property as well as due to their high nonlinearity (for r corresponding to Fig. 2, $\gamma = 114$ W^{-1}km^{-1} and 281W^{-1}km^{-1} for SF6 and SF57 PCFs, respectively), we shall consider only SF6 and SF57 PCFs later.

Figures 3-5 demonstrate the results of the simulations of the SF6 supercontinua. For Fig. 3, the SRS was assumed to be absent ($f = 0$). Figures 4, 5 were calculated, assuming equal Raman contribution $f = 0.13$, but different Raman shift value: 450 cm^{-1} corresponds to a common telecommunication fiber (Fig. 4), 1000 cm^{-1} is the shift in SF6 and SF57 glasses (Fig. 5).

Comparison of Fig. 3 with Fig. 4 shows that, although both the Schrödinger and Raman soliton frequency shifts are almost linearly scalable with the input intensity I_p, SRS provides a wider (approximately in 170 nm for I_p =40 GW/cm^2) spectrum. The dispersion wave (blue-side spike) is input-intensity scalable, as well, but almost independent on SRS.

Doubled, in comparison with common fibers, Raman shift in SF6 (Fig. 5) results in an additional red-shift in comparison with that without SRS (200 nm at the level of I_p =40 GW/cm^2). The most interesting effect in this case is the threshold-like behavior of the red-shift at some level of the input intensity. This causes ≈ 150 nm red extra-broadening at only ≈ 7 GW/cm^2 input level. As a result, the octave-spanning SC is possible already for sub-35 GW/cm^2 input intensities. As it will be demonstrated in the next section, the spectra corresponding to the threshold input intensity possess a maximum coherency.

The red extra-broadening increases with the Raman fraction f. For instance, f =0.19 in SF6 provides more than 200 nm red-shift for 7.5 GW/cm^2 intensity. Thus, such a shift tends to that due to Raman scattering: 1000 cm^{-1} corresponds to ≈260 nm at λ =1.5 μm.

Choice of a more nonlinear glass providing the near-zero GDD in the vicinity of the oscillator spectrum centrum leads to a wider SC. Fig. 6 shows a dependence of the spectrum on the input intensity for the SF57 glass PCF. One can see, that the intensive Raman soliton and the dispersive wave develop and the SRS induced extra-broadening occurs at I_p =5 GW/cm^2. As a result, the octave-spanning SC is possible already at I_p =15 GW/cm^2. An additional fragmentation of the SC central part can be attributed to the stronger third-order dispersion of SF57 in comparison with SF6. It should be noted, that the larger Raman fraction reported in Ref. [26] would provide an additional spectral extra-broadening on the longer-wavelength side of SC.

One has to note the stronger modulation of the Schrödinger soliton spectrum (Fig. 3) in comparison with the Raman soliton one (Figs. 5, 6). This is a general property of the regime under consideration. As the Schrödinger solitons have comparatively small group-delays relatively an input pulse, this results in their interference and causes the spectrum modulation. On the contrary, SRS results in fast formation of a single highly-intensive Raman soliton with a large group-delay (Fig. 7) preventing from the spectrum modulation due to interference. As a result, red-part of the spectrum is more smooth.

5 Spectral coherence of SC

As it was shown in the previous section, SF6 and SF57 glass PCFs allow the octave-spanning SC for low input intensities (35 GW/cm^2 and 15 GW/cm^2, respectively). This is possible due to three factors: i) near-zero GDD at λ =1.5 μm can be provided for the comparatively small mode areas (≈10 μm^2); ii) nonlinear refraction in these glasses is high (γ =114 W^{-1}km^{-1} and 281 W^{-1}km^{-1}, respectively); iii) Raman scattering shift (1000 cm^{-1}) is doubled in comparison with the common fibers.

However, an issue remains: what is the spectral coherence degree, which can be provided by such a highly-nonlinear regime? As it was pointed, a large soliton number N [27] and a modulational instability [28] can cause an essential spectral coherence degradation. Simultaneously, a decrease of pulse width and energy enhances the coherence [17,29]. In this section, stochastic Eq. (2) will be used to analyze the spectral coherence degree [15].

At first, we shall analyze only technical noise that consists of the shot-to-shot pulse intensity fluctuations. In this case, we assume Γ =0 and the white intensity noise. 128 sample input pulses are used to collect the statistics.

Figs. 8, *a* and *b* show, respectively, the averaged spectrum and the coherence degree for 2% input intensity white-noise in SF6 with no SRS. The red spectral part corresponding to the Schrödinger solitons possesses a nearunity coherence. However, this coherence degrades due to spectral modulation caused by an interference between the solitons and the modulational instability complex around λ =1.5 μm. Blue-side of the spectrum produced by the dispersion waves has a smooth near-unity coherence. However, this coherence degrades with the wavelength shortening.

Presence of SRS causes the coherence degradation on the red-side of the spectrum, where the spectral components of the Raman soliton are placed (Fig. 9, *b*). A main source of such a degradation is the Raman soliton jitter [15]: the power-dependence of the soliton group-delay results in fluctuations of the soliton position. Similar but stronger degradation takes a place in SF57, too (PCF 10, *b*).

An obvious way to reduce the coherence degradation due to soliton jitter is to decrease the input intensity [29]. However, the SC spectral width decreases in this case as well (Figs. 5, 6). Most appropriate way is to reduce the PCF length. Fig. 11 shows the spectra from the PCF sections of various lengths. One can see, that already 2 cm section of SF57 PCF provides a sufficiently wide and smooth spectrum. Longer the propagation length does not widen SC essentially but causes its fragmentation. Comparison with Fig. 7 demonstrates that the minimum spectral fragmentation in the 2 cm fiber section corresponds to situation, when the Raman soliton did not yet develop. One can see (Fig. 12, *b*), that in this case the spectral coherence degree is close to 1 almost over all SC. This easily observable parameter (spectral smoothness) can be used for optimization of the SC generation in phase-sensitive applications, without the need to actually measure the degree of coherence.

In order to investigate the maximum degree of coherence, both the quantum source Γ in Eq. (2) and the quantum fluctuations of input field $\Delta\phi$ have to be taken into account. As a source of the input quantum fluctuations, the spontaneous emission in a gain medium are considered [30-33]. When an oscillator operates in the solitonlike regime (as with Cr:YAG), its behavior can be described by the stochastic nonlinear Schrödinger equation with the additive noise term $\Delta\phi$ obeying the correlation [31]:

$$\left\langle \Delta\phi^{*}(0,\omega)\,\Delta\phi\left(0,\omega'\right)\right\rangle = \frac{1}{2\pi\,\bar{n}}\frac{\theta\,\mathrm{K}}{1+\frac{\omega^{2}}{\Delta\omega_{g}^{2}}}G\delta\left(\omega-\omega'\right). \quad (5)$$

Here θ is the enhancement factor due to incomplete inversion of a gain medium, G is the gain coefficient (so that the difference between G and the net-loss coefficient is close to 0), $\Delta\omega_g$ is the gain band-width, K is the Petermann factor [34]. Since $t_0 >> 1/\Delta\omega_g$, the Lorentzian form-factor in Eq. (5) can be omitted. In a Cr:YAG oscillator $\theta \approx 1$ (four-level medium), K ≈1 (small out-put loss [30]) and $G \approx 0.05$ (small net-gain). Last two factors are smaller distinctly than those in a Ti:Sp oscillator. This reduces the quantum noise source $\Delta\phi$ down to 10^{-5} in our dimensionless units for I_p =40 GW/cm^2, t_0=34 fs (the pulse is centered at λ =1.5 μm). This value is below the input vacuum noise in the Wigner representation [21]:

$$\left\langle \Delta\phi^{*}(0,\tau)\,\Delta\phi\left(0,\tau'\right)\right\rangle = \frac{1}{2\,\bar{n}}\delta\left(\tau-\tau'\right). \quad (6)$$

The Raman noise source in Eq. (2) obeys [21,24]:

$$\left\langle \Gamma(\zeta,\omega)\Gamma\left(\zeta',\omega\right)\right\rangle = \frac{1}{n}\left[n_{th}(|\omega|)+\frac{1}{2}\right]\alpha(|\omega|)\delta\left(\zeta-\zeta'\right)\delta\left(\omega+\omega'\right), \quad (7)$$

where n_{th} is the phonon thermal Bose distribution and α is the Raman gain. The relative contribution of the Raman noise term is of order of 10^{-3}. Thus, this noise dominates in our case.

Figs. 8-10, 12 demonstrate the maximum degree of coherence, which is defined by the quantum noises given by Eqs. (5-7). One can see, that the dominating Raman noise does not produce a coherence degradation in our case (compare Figs. 8 and 9). This can be explained by the fact that the input quantum noise is strongly suppressed for Cr:YAG oscillator, the pulse width is <100 fs [17] and the soliton fission occurs over a short propagation distance [27].

Thus, the dominating source of the coherence degradation is the technical shot-to-shot noise. However, as it was demonstrated, its influence can be suppressed by shortening of the PCF section down to ≈2 cm without some essential decrease of the SC width.

Interesting property of the regime under consideration is that the spectral coherence is close to unity in the vicinity of the threshold input intensities. This can be explained in the following way. The threshold-like spectral extra-broadening on the red side of SC results from the large Raman shift (≈1000 cm^{-1}), which scatters the spectral components out-side an initial spectrum. Simultaneously, the coherence between this components and initial (coherent) spectrum remains.

To compare the properties of this regime with the soliton self-frequency shift [11], let us consider the influence of the technical shot-to-shot noise on Raman solitons propagating in a long section (1.5 m) of the dispersion-flattened high-nonlinearity silica fiber under excitation by the high-energy (1 nJ) 80 fs pulses centered at 1.06 μm (parameters correspond to those given in Ref. [11]). Fig. 13 shows the averaged spectrum (black curve, *a*), a single-shot spectrum (gray curve, *b*), as well as the degree of spectral coherence (*b*). One can see, that there may be more than one Raman solitons between 1.3 and 1.7 μm (gray curve, *a*). Their spectral and timing jitters are very strong. This causes a significant spectral broadening of the averaged spectrum (black curve, *a*), but at the expense of a catastrophical degradation of the spectral coherence (*b*). The sources of this phenomena are i) high value of E (note, that the self-frequency shift scales as E^4) and ii) very long propagation distance L. We thus conclude that the Raman soliton approach to spectral broadening is counterproductive, if coherence is an issue.

6 Conclusion

Raman effects on octave-spanning SC from the highly-nonlinear-glass (SF6 and SF57) PCFs have been investigated numerically. The measured Raman gain spectra have demonstrated over twice as high Raman shift in these glasses in comparison with that in the fused silica. It was found that such a shift causes the spectral extra-broadening ($\approx 150 \div 260$ nm) that provides an octave-spanning SC at the extremely low input intensity level (≈35 GW/cm^2 for SF6 and ≈15 GW/cm^2 for SF57). Such low intensity levels allow using the high-repetition rate femtosecond all-solid-state Cr:YAG oscillators, which operates at relatively low output coupling and pulse energy. As a result, the quantum noise at fiber input can be significantly reduced.

Europe PMC Funders Author Manuscripts

The dependence of the SC width on the input intensity has a threshold-like character. Although numerical analysis demonstrated that the spectral coherence degrades with the pulse intensity growth due to Raman soliton jitter, the coherence is close to unity in the vicinity of the threshold intensity due to coupling of the red-side spectral component provided by a large Raman shift.

It was found, that the dependence of the SC coherence and width on the propagation length is threshold-like, as well. There exists an optimum fiber length, which provides the broad SC spectrum without compromising coherence properties. The high coherence in this case corresponds to initial stage of the Raman soliton formation, when the jitter does not develop yet. It was found, that the high spectral coherence in this regime correlates with the smoothness of the spectrum, giving an easy observable optimization criterium. This property allows broad application of Raman-assisted SC generators in phase-controlled setups.

Acknowledgments

This work has been performed under Austrian Fonds zur Förderung der Wissenschaftlichen Forschung Grant No. P17973.

References

1. Holzwarth RH, Udem T, Hänsch TW, Knight JC, Wadsworth WJ, Russell PSJ. Phys. Rev. Lett. 2000; 85:2264. [PubMed: 10977987]
2. Jones DA, Diddams SA, Ranka JK, Stentz A, Windeler RS, Hall JL, Cundiff ST. Scince. 2000; 288:635.
3. Baltuska A, Wei Z, Pschenichnikov MS, Wiersma DA, Szipocs R. Appl. Phys. B. 1997; 65:175.
4. Alfano, RR., editor. The supercontinuum laser sorce. Springer-Verlag; New York: 1989.
5. Russell P. Nature. 2003; 299:358.
6. Agrawal, GP. Nonlinear fiber optics. Academic Press; San Diego: 2001.
7. Herrmann J, Griebner U, Zhavoronkov N, Husakov A, Nickel D, Knight JC, Wadsworth WJ, Russell PSJ, Korn G. Phys. Rev. Lett. 2002; 88:173901. [PubMed: 12005754]
8. Kalashnikov VL, Sorokina E, Naumov S, Sorokina IT, Ravi Kanth Kumar VV, George AK. Appl. Phys. B. 2004; 79:591.
9. Nishizava N, Goto T. Jpn. J. Appl. Phys. 2001; 40:L365.
10. Saitoh K, Koshiba M. Opt. Express. 2004; 12:2027. [PubMed: 19475038]
11. Chen, J.; Ilday, FÖ.; Kärtner, FX. ASSP
12. Ravi Kanth Kumar VV, George AK, Reeves WH, Knight JC, Russell PSJ, Omenetto FG, Taylor AJ. Opt. Express. 2002; 10:1520. [PubMed: 19461687]
13. Hundertmark H, Kracht D, Wandt D, Fallnich C, Ravi Kanth Kumar VV, George AK, Knight JC, Russell PSJ. Opt. Express. 2003; 11:3196. [PubMed: 19471445]
14. Cristiani I, Tediosi R, Tartara L, Degiorgio V. Opt. Express. 2004; 12:124. [PubMed: 19471518]
15. Dudley JM, Coen S. Opt. Lett. 2002; 27:1180. [PubMed: 18026400]
16. Corwin KL, Newbury NR, Dudley JM, Coen S, Diddams SA, Weber K, Windeler RS. Phys. Rev. Lett. 2003; 90:113904. [PubMed: 12688929]
17. Corwin KL, Newbury NR, Dudley JM, Coen S, Diddams SA, Washburn BR, Weber K, Windeler RS. Appl. Phys. B. 2003; 77:269.
18. Naumov S, Sorokin E, Kalashnikov VL, Tempea G, Sorokina IT. Appl. Phys. B. 2003; 76:1.
19. Lai Y, Haus HA. Phys. Rev. A. 1989; 40:844. [PubMed: 9902211]
20. Lee H-W. Phys. Rep. 1995; 259:147.
21. Carter SJ. Phys. Rev. A. 1995; 51:3274. [PubMed: 9911968]
22. Drummond PD, Corney JF. J. Opt. Soc. Am. B. 2001; 18:139.
23. Kärtner FX, Dougherty DJ, Haus HA, Ippen EP. J. Opt. Soc. Am. B. 1994; 11:1267.

24. Corney JF, Drummond PD. J. Opt. Soc. Am. B. 2001; 18:153.
25. Kibler B, Dudley JM, Coen S. Appl. Phys. B. 2005; 81:337.
26. Leong JYY, Petropoulos P, Price JHV, Ebendorff-Heidepriem H, Asimakis S, Moore RC, Frampton KE, Finazzi V, Feng X, Monro TM, Richardson DJ. J. Lightwave Tech. 2006; 24:183.
27. Gu X, Kimmel M, Shreenath AP, Trebino R, Dudley JM, Coen S, Windeler RS. Opt. Express. 2003; 11:2697. [PubMed: 19471384]
28. Lu F, Knox WH. Opt. Express. 2004; 12:347. [PubMed: 19471544]
29. Washburn BR, Newbury NR. Opt. Express. 2004; 12:2166. [PubMed: 19475052]
30. Siegman AE. Phys. Rev. A. 1989; 39:1264. [PubMed: 9901362]
31. Haus HA. J. Opt. Soc. Am. B. 1991; 8:1122.
32. Haus HA. IEEE J. Quantum Electr. 1993; 29:983.
33. Haus HA, Margalit M, Yu CX. J. Opt. Soc. Am. B. 2000; 17:1240.
34. Henry CH, Kazarinov RF. Rev. Mod. Phys. 1996; 68:801.
35. Pantell, PH.; Puthoff, HE. Fundamentals of quantum electronics. Wiley: 1969.
36. Johnston WD, et al. Appl. Phys. Lett. 1968; 13:190.
37. Stolen RH, Ippen EP. Appl. Phys. Lett. 1973; 22:276.
38. Sorokina IT, Sorokin E, Wintner E, Cassanho A, Jenssen HP. OSA Trends in Optics and Photonics. 1998; 19:359.
39. Rivero C, Stegeman R, Couzi M, Talaga D, Cardinal T, Richardson K, Stegeman G. Opt. Express. 2005; 13:4759. [PubMed: 19495394]
40. Heiman D, Hellwarth RW, Hamilton DS. J. Non-Cryst. Solids. 1979; 34:63.

Europe PMC Funders Author Manuscripts

Europe PMC Funders Author Manuscripts

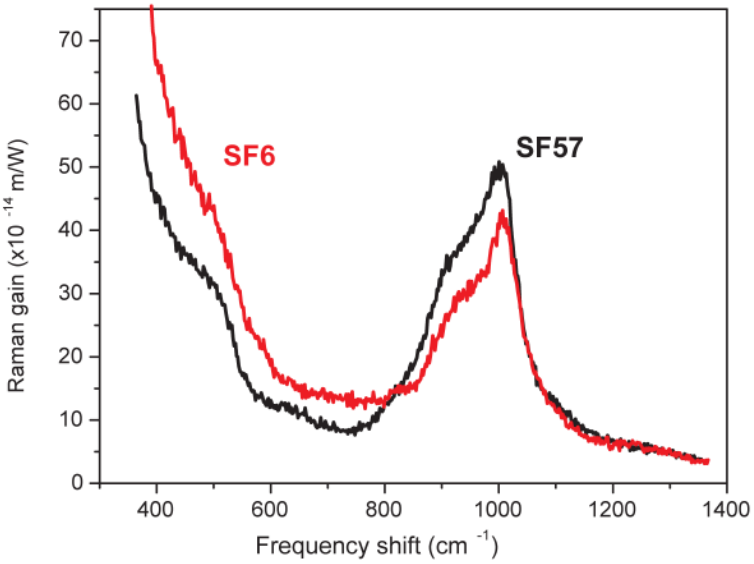

Fig. 1.
Calibrated Raman gain spectra (parallel polarization) of nonlinear heavy flint glasses SF6 and SF57. The increase of the signal on the low-frequency side of spectra is caused by the strong Raleigh wing in the 180° recording geometry

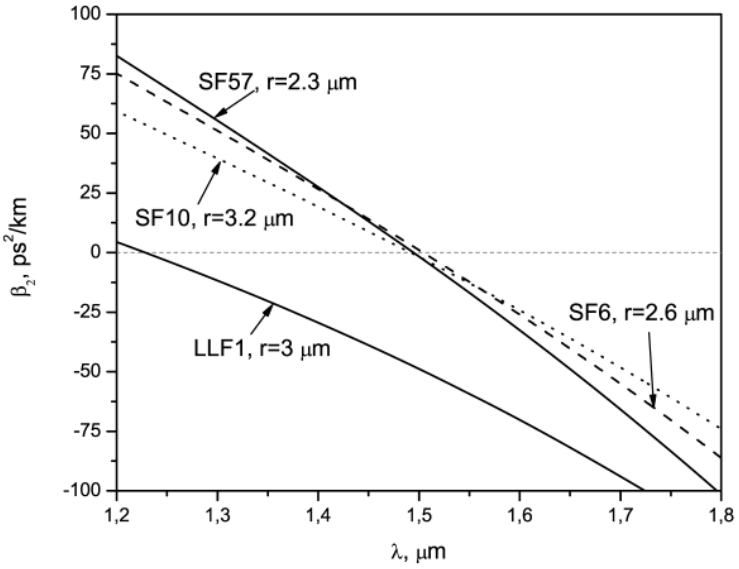

Fig. 2.
Wavelength dependence of GDD for the different glasses. *r* is the cylindrical core radius.

Europe PMC Funders Author Manuscripts

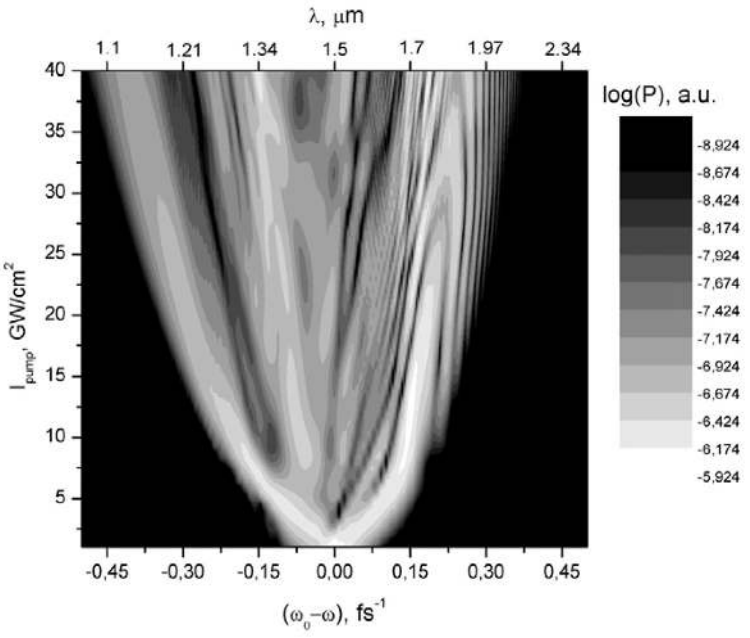

Fig. 3.

Contour-plot of logarithm of the spectral power *P* vs. the input pulse power for the SF6 PCF. SRS does not taken into account (*f*=0). 20 cm propagation length.

Europe PMC Funders Author Manuscripts

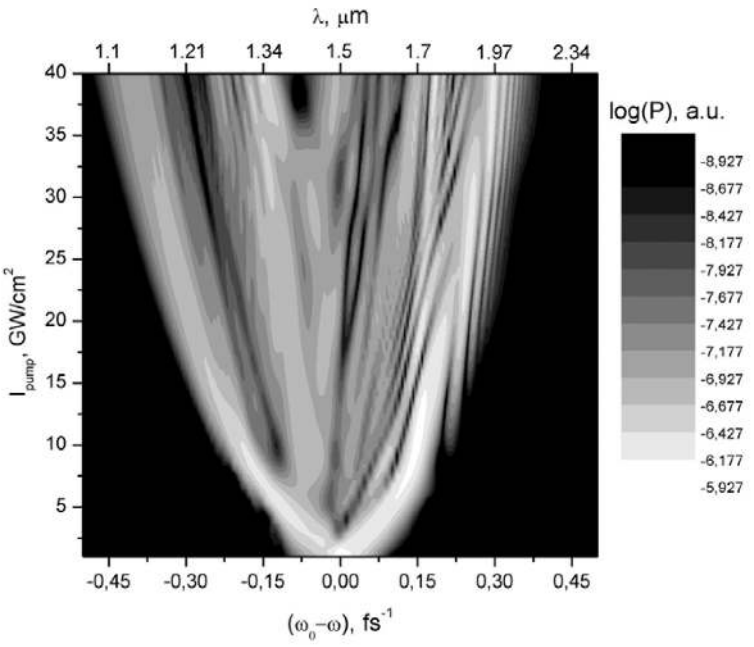

Fig. 4.

Contour-plot of logarithm of the spectral power P vs. the input pulse power for the SF6 PCF. Raman shift is 450 cm^{-1} (f=0.13). 20 cm propagation length.

Europe PMC Funders Author Manuscripts

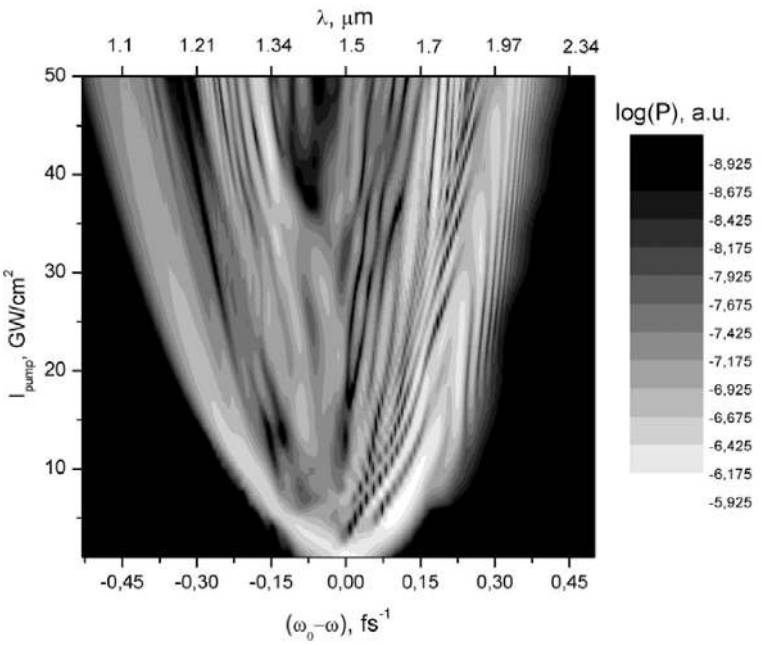

Fig. 5.

Contour-plot of logarithm of the spectral power *P* vs. the input pulse power for the SF6 PCF. Raman shift is 1000 cm^{-1} (f=0.13). 20 cm propagation length.

Europe PMC Funders Author Manuscripts

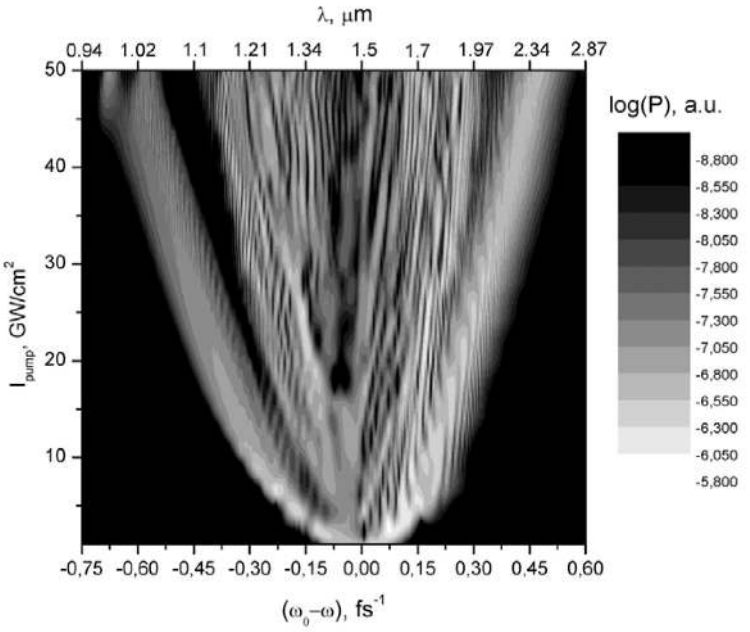

Fig. 6.

Contour-plot of logarithm of the spectral power *P* vs. the input pulse power for the SF57 PCF. Raman shift is 1000 cm^{-1} (f=0.1). 20 cm propagation length.

Europe PMC Funders Author Manuscripts

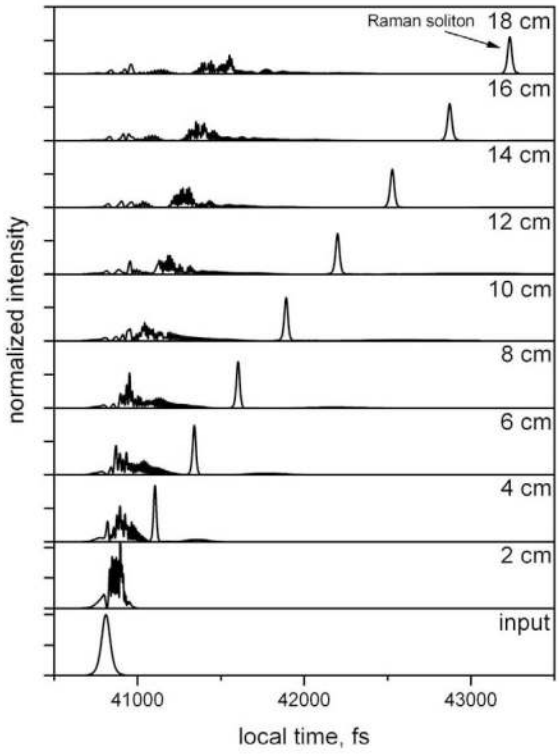

Fig. 7.
Normalized intensity profiles from the SF57 PCF sections of various lengths (showed in figures). I_p =40 GW/cm^2.

Europe PMC Funders Author Manuscripts

Europe PMC Funders Author Manuscripts

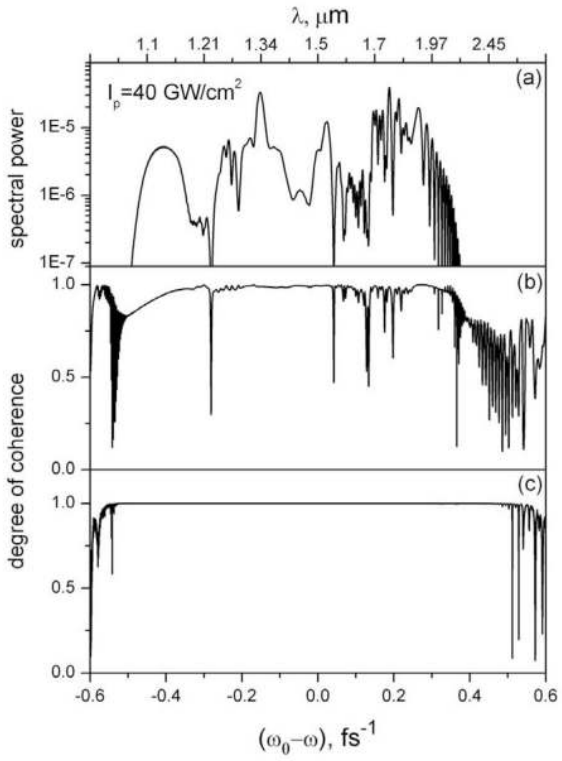

Fig. 8.

Averaged spectrum (*a*), degree of coherence (*b*) for 2% input power fluctuations and coherence quantum limit (*c*). 20 cm section of SF6 glass PCF, I_p =40 GW/cm^2, no SRS.

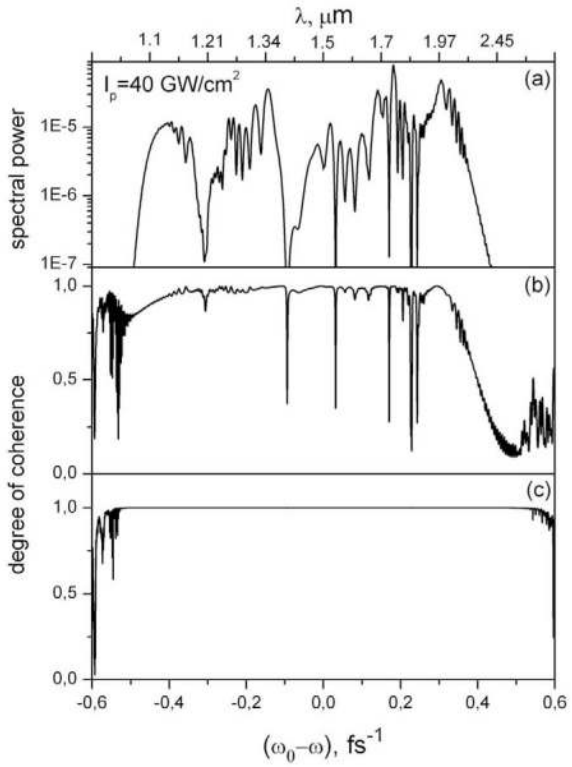

Fig. 9.

Averaged spectrum (*a*), degree of coherence (*b*) for 2% input power fluctuations and coherence quantum limit (*c*). 20 cm section of SF6 glass PCF with SRS, I_p =40 GW/cm^2.

Europe PMC Funders Author Manuscripts

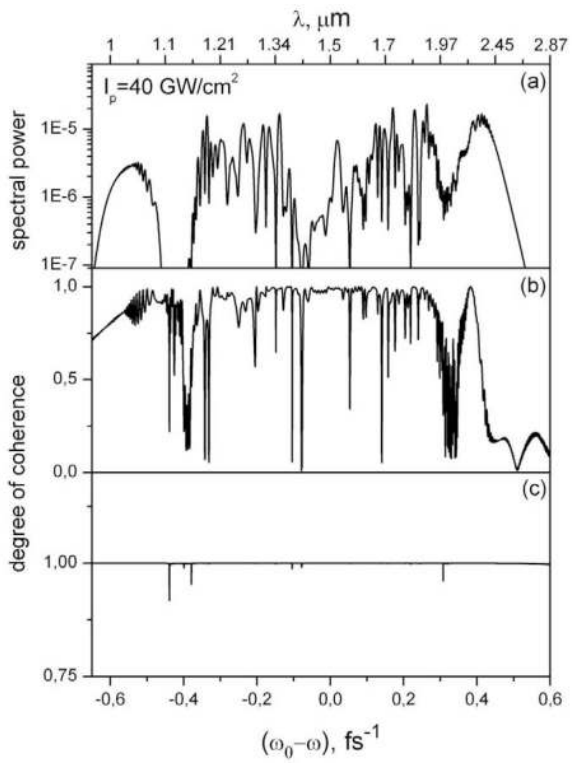

Fig. 10.

Averaged spectrum (*a*), degree of coherence (*b*) for 2% input power fluctuations and coherence quantum limit (*c*). 20 cm section of SF57 glass PCF with SRS, I_p =40 GW/cm^2.

Europe PMC Funders Author Manuscripts

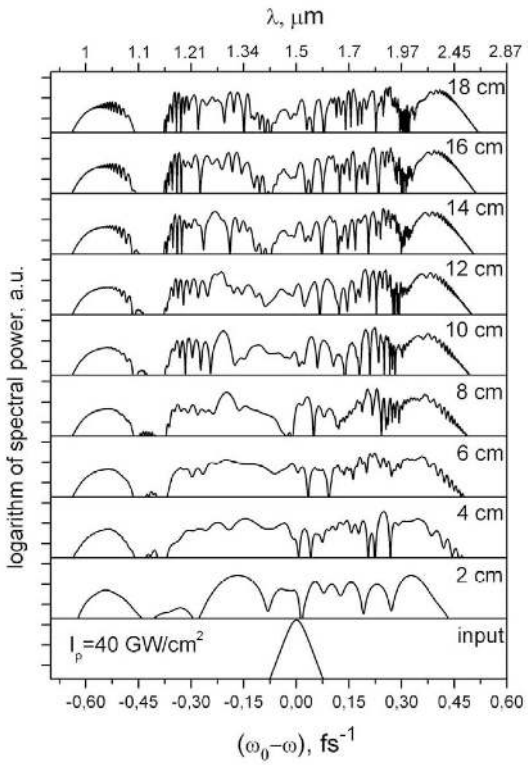

Fig. 11.
Normalized spectra from the SF57 PCF sections of various lengths (showed in figures). I_p =40 GW/cm^2.

Europe PMC Funders Author Manuscripts

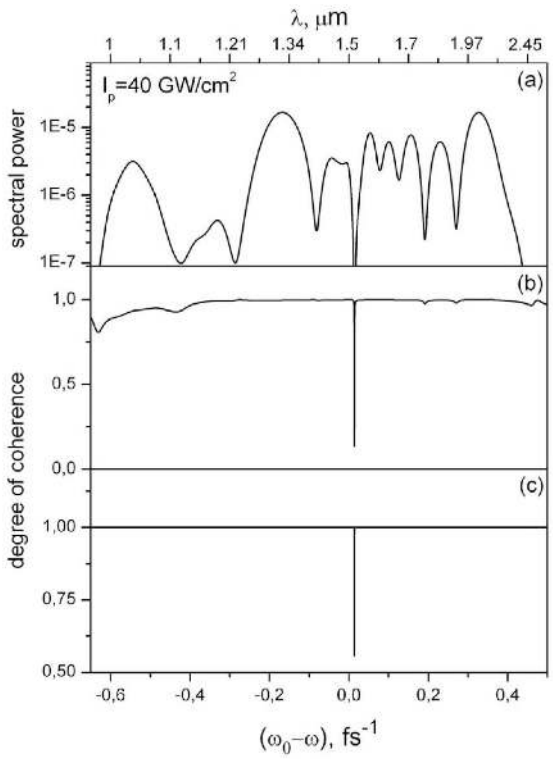

Fig. 12.

Averaged spectrum (*a*), degree of coherence (*b*) for 2% input power fluctuations and coherence quantum limit (*c*). 2 cm section of SF57 glass PCF with SRS, I_p =40 GW/cm^2.

Europe PMC Funders Author Manuscripts

Europe PMC Funders Author Manuscripts

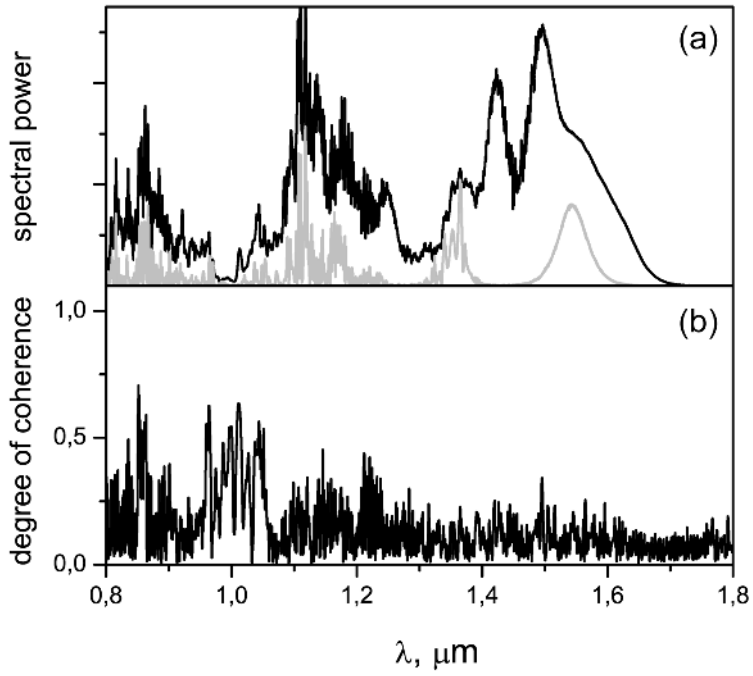

Fig. 13.

Averaged spectrum (*a*, black), single-shot spectrum (*a*, gray) and degree of coherence (*b*) for 2% input power fluctuations for the soliton self-frequency shift regime. 150 cm section of the dispersion-flattened fiber with an enhanced nonlinearity, I_p =21 GW/cm^2, β_2 =−80 fs^{2}cm^{-1}, β_3 =−1222 fs^{3}cm^{-1}, γ =25 W^{-1}km^{-1}.

Europe PMC Funders Author Manuscripts

Table 1

Raman gain parameters of nonlinear glasses, in comparison with fused silica.

Material	n_2	Peak Raman gain at 1.5 μm	Peak position	Peak width	f
SF6	21×10^{-16} cm^2/W	40×10^{-14} m/W	1010 cm^{-1}	200 cm^{-1}	0.1
SF57	41×10^{-16} cm^2/W	50×10^{-14} m/W	1000 cm^{-1}	200 cm^{-1}	0.13
Fused Silica	3×10^{-16} cm^2/W	3.5×10^{-14} m/W	450 cm^{-1}	200 cm^{-1}	0.19

Appl Phys B. Author manuscript; available in PMC 2010 October 21.